International Journal of Solids and Structures 262–263 (2023) 112075

Contents lists available at ScienceDirect

International Journal of Solids and Structures

journal homepage: www.elsevier.com/locate/ijsolstr

Wrinkling of twisted thin films

Fan-Fan Wang [a,1], Ting Wang [b,1], Xiaoliang Zhang [b], Yangchao Huang [b], Ivan Giorgio [c], Fan Xu [b,*]

[a] School of Mathematics, East China University of Science and Technology, Shanghai 200237, PR China
[b] Institute of Mechanics and Computational Engineering, Department of Aeronautics and Astronautics, Fudan University, Shanghai 200433, PR China
[c] Department of Civil, Construction-Architectural and Environmental Engineering (DICEAA), University of L'Aquila, L'Aquila, Italy

ARTICLE INFO

Keywords:
Wrinkling
Twist
Bifurcation
Finite-strain plate model
Thin films

ABSTRACT

Thin films usually exhibit instabilities and yield intricate wrinkles when two clamped ends are twisted. Here, we explore the wrinkling behavior and pitch-fork bifurcation of twisted thin films experimentally and theoretically. To quantitatively predict the post-buckling evolution of twist-induced wrinkling morphology, we develop a refined finite-strain plate model derived from 3D field equations and then solve it by using the finite element method with COMSOL. We examine the effects of aspect ratios and pre-tension on the wrinkling profile. We reveal three distinguished wrinkling evolution regimes depending on the aspect ratios of thin films as the twisting angle increases: (a) wrinkles initially occur at both free ends of the film and then develop toward the center; (b) wrinkles appear at the center and then develop toward both free ends; (c) wrinkles emerge at the center and are localized therein. The increase of film thickness and pre-stretch can strengthen the film stiffness and thus increase the critical twisting threshold, resulting in the prevention of wrinkle formation. Understanding the morphological pattern evolution of twisted films may guide rational designs of wrinkle-tunable membrane surfaces and structures.

1. Introduction

Thin films and plates usually have small bending stiffness and thus, under external stimuli, some local buckling, *i.e.*, wrinkling, would occur inevitably on the surface. In the experiments by Wong and Pellegrino (2006), wrinkles emerge when a rectangular membrane is subjected to simple shear and a square membrane is subjected to two pairs of equal in magnitude and opposite diagonal forces at the corners. Transverse wrinkles perpendicular to the uniaxial stretching direction appear in rectangular membranes and can disappear upon excess stretching (Zheng, 2009; Nayyar et al., 2011; Healey et al., 2013; Sipos and Fehér, 2016; Li and Healey, 2016; Wang et al., 2019a, 2022b).

Compared with the stretch-induced wrinkling of thin films, instabilities of twisted thin membranes are also omnipresent in our daily life and modern industry (see Fig. 1), showing intriguing wrinkling patterns yet receiving less attention. Elastic instability of a thin twisted strip (thin plate with a large aspect ratio) was first studied by Green (1936, 1937). The thin strip becomes unstable and buckles into a helical configuration together with a wavy form at a finite twisting angle. Most early works on the twisted plates focused on the critical twisting threshold and instability modes. In Chopin and Kudrolli (2013), different instability modes, including longitudinal and transverse buckling, creased helicoid and loop were experimentally observed in elastic ribbons upon tension–twist. It was revealed that transverse wrinkles occur in a twisted ribbon with a large aspect ratio under high tension. In Kudrolli and Chopin (2018), three different transverse instabilities corresponding to three regimes with increasing aspect ratios were identified, *i.e.*, a clamped-dominated regime, a bendable regime, and a stiff regime. In Chopin and Romildo Filho (2019), experiments on significant twist and tension of soft ribbons were carried out and Föppl–von Kármán (FvK) equations were used to model the evolution of longitudinal strain and torque.

Theoretical investigations on twisted films/plates were generally based on specific plate theories. Green (1937) applied a weakly nonlinear plate theory and thus, the twisting angle remains small. In Crispino and Benson (1986), the twist instability of orthotropic rectangular plates was explored based on the Föppl–von Kármán orthotropic plate equations. In Goriely et al. (2001), dynamics of twisted straight strips with noncircular cross sections were analyzed based on the dynamic Kirchhoff equations by using a perturbation scheme. Based on a fully nonlinear plate theory, Mockensturm (2001) showed that the twisted end conditions could affect the buckling modes and critical twisting angles. In Coman and Bassom (2008), adopting the nonlinear Donnell–von Kármán equations based on the assumption that the transverse

* Corresponding author.
E-mail address: fanxu@fudan.edu.cn (F. Xu).
[1] These authors contributed equally to this work.

https://doi.org/10.1016/j.ijsolstr.2022.112075
Received 18 September 2022; Received in revised form 1 December 2022; Accepted 2 December 2022
Available online 5 December 2022
0020-7683/© 2022 Elsevier Ltd. All rights reserved.

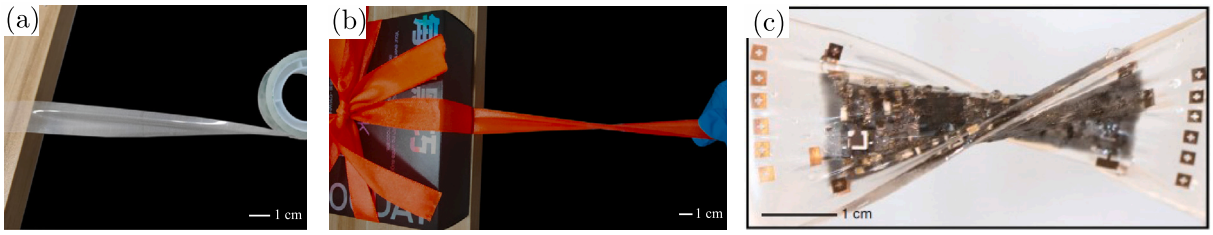


Fig. 1. Twist-induced wrinkles are ubiquitous in our daily life and modern industry. (a) Adhesive strip. (b) Packing belt. (c) Integrated flexible electronics (Huang et al., 2018).

deflections remain small in comparison with the in-plane dimensions of the plate, elastic instability was explored when the thin plates are subjected to slight twisting and initial tensile force at both short edges. In Chopin et al. (2015), which is a subsequent theoretical work of the experiments in Chopin and Kudrolli (2013), from the covariant form of the Föppl von–Kármán (cFvK) equations, a phase diagram for different types of instabilities of a stretched and twisted ribbon was constructed in terms of tension, twist, length and thickness of the ribbon. Pertaining to the experiments in Chopin and Kudrolli (2013), a theoretical treatment was performed for the wrinkling of a twisted ribbon in Kohn and O'Brien (2018). Lately, Faghfouri and Rammerstorfer (2020) numerically investigated mode transitions of a twisted ribbon under tension. Nevertheless, how do wrinkles evolve in twisted thin films and what are the key factors on pattern selection remain elusive.

Here, we explore, both experimentally and theoretically, the intricate evolutions of transverse wrinkling of twisted thin films, from a flat configuration to the onset of wrinkling, and the further development of wrinkling patterns as the twisting angle increases. To quantitatively understand the underlying mechanism and to precisely predict the post-buckling evolution of twist-induced wrinkling morphology, we develop a refined finite-strain plate model based on the method of coupled series-asymptotic expansions (Dai and Cai, 2006; Dai and Wang, 2012; Dai et al., 2013, 2015). For most existing plate theories, some *ad hoc* kinematic and/or scaling assumptions are usually needed, such as Kirchhoff–Love hypothesis. Within the well-known FvK plate theory, it is assumed that the thickness does not change and the in-plane strain does not affect the bending energy. In the commercial software package Abaqus, a shell element S4R is claimed to be suitable for general thin-walled structures. Then, a risk may arise, to what extent, these hypotheses do not affect the reliability of the results, in particular, in the post-buckling regime. We show that the refined finite-strain plate model developed here without any assumption can precisely predict the twist-induced wrinkling morphology of thin films at finite strain. We elucidate the effects of aspect ratios and pre-tension on the wrinkling profile. We demonstrate that the transverse wrinkling of twisted films experiences a pitch-fork bifurcation. We reveal three distinguished evolution regimes of transverse wrinkles with the rise of the twisting angle. Eventually, we draw a phase diagram to provide an overall view of the interactive effects of aspect ratios on the wrinkling morphology of twisted thin films.

The paper is organized as follows. In Section 2, we illustrate an experimental setup to explore twist-induced wrinkling of thin films. In Section 3, we formulate the refined finite-strain plate model and the weak forms for an incompressible neo-Hookean plate. In Section 4, we examine the effects of aspect ratios and the pre-stretch on wrinkling scenarios and further provide a phase diagram on pattern selection.

2. Experiment

We perform experiments to explore the wrinkling behavior of twisted membranes. Polydimethylsiloxane (PDMS) film made by Bald Advanced Materials Ltd. is used, with elastic modulus $E = 2.3$ MPa and nominal thickness $t = 50$ μm, which holds an ultimate stretching strain over 400% and is fully elastic in the strain range for the observations in this work. The 3D printing technology facilitates producing flat heads made of poly lactic acid (PLA), and then the films are firmly glued to the heads by 3M double-sided tapes. The film is completely fixed on the upper end and can be rotated on the bottom head, while two vertical edges of the film are set free. Fig. 2 shows that two packets of transverse wrinkles initially emerge around free sides (at twisting angle $\theta = 0.5$) and then spread toward the center with the increase of twisting angle ($\theta = 0.74$). Eventually, transverse wrinkles cover the entire width.

3. A refined finite-strain plate model

To quantitatively predict the onset and post-buckling evolution of twist-induced wrinkling behavior of thin films, we derive a refined finite-strain plate model based on the consistent plate theory (Dai and Song, 2014; Wang et al., 2016). In Wang et al. (2019b), a uniformly-valid plate equation was derived and the corresponding weak form was provided. In Wang et al. (2022a), from the corresponding weak forms, numerical simulations for a plate subjected to uniform loadings on the top of the plate were performed. For completeness, here we present the formulation of the consistent finite-strain plate theory and one can refer to Wang et al. (2019b, 2022a) for more details.

As shown in Fig. 2(a), we take the Cartesian coordinate system, where $\mathbf{X} = (X, Y, Z)$ and $\mathbf{x} = \mathbf{x}(X, Y, Z)$ denote the position vectors of a material point in the reference and the current configurations, respectively. The width, length, and thickness of the plate are represented by W, L, and $t = 2h$, respectively. We introduce two aspect ratios for the plate, *i.e.*, length-to-width ratio $\beta = L/W$ and width-to-thickness ratio $\alpha = W/t$, where α could be very large for ultrathin films.

We assume that the film is composed of incompressible material with the strain energy function ψ. The incompressibility constraint reads

$$R(\mathbf{F}) = \det\mathbf{F} - 1 = 0, \tag{3.1}$$

and the nominal stress $\mathbf{S}$ is given by

$$\mathbf{S} = \frac{\partial\psi}{\partial\mathbf{F}} - p\frac{\partial R}{\partial\mathbf{F}}, \tag{3.2}$$

where $\mathbf{F}$ is the deformation gradient tensor and p is the Lagrange multiplier.

Neglecting body forces, we start from the three-dimensional field equations

$$\mathrm{Div}\,\mathbf{S} = \mathbf{0}. \tag{3.3}$$

The top and bottom surfaces of the plate are traction free and then we have

$$\mathbf{S}^{\mathrm{T}}\mathbf{k}|_{Z=0,2h} = \mathbf{0}, \tag{3.4}$$

where $\mathbf{k}$ is the upward unit normal of the top surface of the film.

The key point of the consistent finite-strain plate theory is that the series expansions of the placement vector $\mathbf{x}$, deformation gradient tensor $\mathbf{F}$, nominal stress tensor $\mathbf{S}$ and hydrostatic pressure p are respectively expanded about the bottom surface of the plate,

$$\mathbf{x} = \mathbf{x}^{(0)} + Z\mathbf{x}^{(1)} + \frac{1}{2}Z^2\mathbf{x}^{(2)} + \frac{1}{3!}Z^3\mathbf{x}^{(3)} + \frac{1}{4!}Z^4\mathbf{x}^{(4)} + \mathcal{O}(Z^5), \tag{3.5}$$

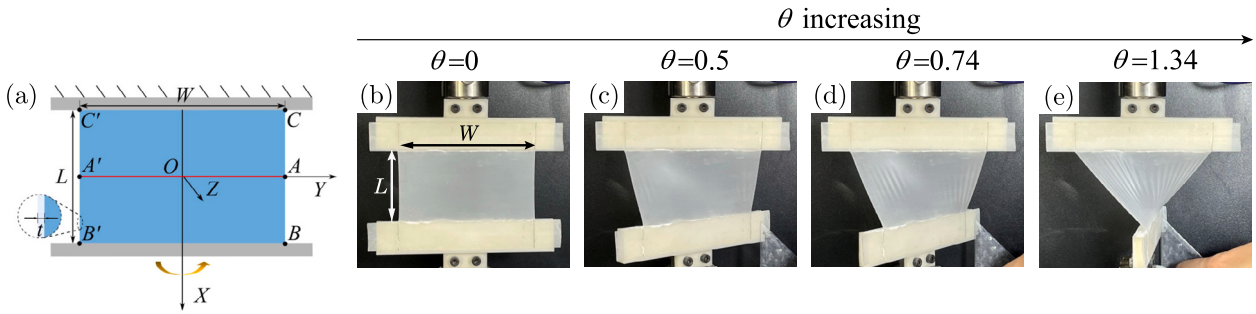


Fig. 2. Transverse wrinkles initially occur near both free edges and then develop toward the center with the increase of twisting angle θ: (a) sketch of a twisting thin film and the coordinate system, (b) $\theta = 0$, smooth, (c) $\theta = 0.5$, wrinkling near free edges, (d) $\theta = 0.74$, wrinkles spread toward the center, (e) $\theta = 1.34$, wrinkles cover the entire film. The film dimensions read $W = 100$ mm, $L = 50$ mm and $t = 50$ μm.

$$\mathbf{F} = \mathbf{F}^{(0)} + Z\mathbf{F}^{(1)} + \frac{1}{2}Z^2\mathbf{F}^{(2)} + \frac{1}{3!}Z^3\mathbf{F}^{(3)} + \mathcal{O}(Z^4), \tag{3.6}$$

$$\mathbf{S} = \mathbf{S}^{(0)} + Z\mathbf{S}^{(1)} + \frac{1}{2!}Z^2\mathbf{S}^{(2)} + \frac{1}{3!}Z^3\mathbf{S}^{(3)} + \mathcal{O}(Z^4), \tag{3.7}$$

$$p = p^{(0)} + Zp^{(1)} + Z^2p^{(2)} + \mathcal{O}(Z^3), \tag{3.8}$$

where we have assumed sufficient smoothness for the coefficient functions.

We note that

$$\mathbf{F}^{(i)} = \nabla\mathbf{x}^{(i)} + \mathbf{x}^{(i+1)} \otimes \mathbf{k}, \quad i = 0, 1, 2, 3, \tag{3.9}$$

where $\nabla(\cdot)$ and $\otimes$ denote the surface gradient and the tensor product, respectively.

The field Eq. (3.3) together with the above expansion (3.7) lead to the recursive relations for the stress coefficients

$$\nabla \cdot \mathbf{S}^{(0)} + (\mathbf{S}^{(1)})^{\mathrm{T}}\mathbf{k} = \mathbf{0}, \tag{3.10}$$

$$\nabla \cdot \mathbf{S}^{(1)} + (\mathbf{S}^{(2)})^{\mathrm{T}}\mathbf{k} = \mathbf{0}, \tag{3.11}$$

$$\nabla \cdot \mathbf{S}^{(2)} + (\mathbf{S}^{(3)})^{\mathrm{T}}\mathbf{k} = \mathbf{0}. \tag{3.12}$$

The top and the bottom traction-free conditions (3.4) together with the series expansion (3.7) yield

$$(\mathbf{S}^{(0)})^{\mathrm{T}}\mathbf{k} + 2h(\mathbf{S}^{(1)})^{\mathrm{T}}\mathbf{k} + \frac{1}{2}(2h)^2(\mathbf{S}^{(2)})^{\mathrm{T}}\mathbf{k} + \frac{1}{3!}(2h)^3(\mathbf{S}^{(3)})^{\mathrm{T}}\mathbf{k} + \mathcal{O}(h^4) = \mathbf{0}, \tag{3.13}$$

$$(\mathbf{S}^{(0)})^{\mathrm{T}}\mathbf{k} = \mathbf{0}. \tag{3.14}$$

Note that three equations in (3.14) provide three algebraic equations for solving $\mathbf{x}^{(1)}$ in terms of $\nabla\mathbf{x}^{(0)}$. For general hyperelastic material, (3.14) are three nonlinear algebraic equations of $\mathbf{x}^{(1)}$, and they become three linear algebraic equations of $\mathbf{x}^{(1)}$ for incompressible neo-Hookean material and then $\mathbf{x}^{(1)}$ can be solved in terms of $\nabla\mathbf{x}^{(0)}$ explicitly.

Subtraction of (3.13) and (3.14), by using (3.10)–(3.12), yields

$$\nabla \cdot \mathbf{S}^{(0)} + h\nabla \cdot \mathbf{S}^{(1)} + \frac{2}{3}h^2\nabla \cdot \mathbf{S}^{(2)} + \mathcal{O}(h^3) = \mathbf{0}. \tag{3.15}$$

The above equation can be rewritten as the combination of two parts

$$\nabla \cdot \mathbf{S}_t^{(0)} + h\nabla \cdot \mathbf{S}_t^{(1)} + \frac{2}{3}h^2\nabla \cdot \mathbf{S}_t^{(2)} + \mathcal{O}(h^3) = \mathbf{0}, \tag{3.16}$$

$$\nabla \cdot (\mathbf{S}^{(0)}\mathbf{k}) + h\nabla \cdot (\mathbf{S}^{(1)}\mathbf{k}) + \frac{2}{3}h^2\nabla \cdot (\mathbf{S}^{(2)}\mathbf{k}) + \mathcal{O}(h^3) = 0, \tag{3.17}$$

where the quantities (3.16) with subscript t denotes the corresponding in-plane part.

From (3.15), upon using (3.14), (3.10) and (3.11) (or simply adding (3.13) and (3.14)), one obtains

$$(\mathbf{S}^{(0)})^{\mathrm{T}}\mathbf{k} + h(\mathbf{S}^{(1)})^{\mathrm{T}}\mathbf{k} + h^2(\mathbf{S}^{(2)})^{\mathrm{T}}\mathbf{k} + \mathcal{O}(h^3) = \mathbf{0}. \tag{3.18}$$

Through the manipulation (3.17) $-\nabla\cdot$ (3.18), upon using (3.11) and (3.12), one obtains

$$\begin{aligned}&\nabla \cdot \left(\mathbf{S}^{(0)}\mathbf{k} - (\mathbf{S}^{(0)})^{\mathrm{T}}\mathbf{k}\right) + h\nabla \cdot \left(\mathbf{S}^{(1)}\mathbf{k} - (\mathbf{S}^{(1)})^{\mathrm{T}}\mathbf{k}\right)\\ &+\frac{2}{3}h^2\nabla \cdot \left(\mathbf{S}^{(2)}\mathbf{k} - (\mathbf{S}^{(2)})^{\mathrm{T}}\mathbf{k}\right)\\ &+\frac{1}{3}h^2\nabla \cdot \nabla \cdot \mathbf{S}_t^{(1)} + \mathcal{O}\left(h^3\right) = 0.\end{aligned} \tag{3.19}$$

The consistent finite-strain asymptotic plate Eqs. (3.16) and (3.19) are three equations for the unknown $\mathbf{x}^{(0)}$ with $\mathbf{x}^{(1)}$, $\mathbf{x}^{(2)}$ and $\mathbf{x}^{(3)}$ being obtained from linear algebraic Eqs. (3.14), (3.10) and (3.11), respectively.

For the purpose of finite element analysis, proper weak forms need to be formulated. Removing the higher order terms in (3.16) and (3.19), multiplying both sides by the virtual displacements $\delta\boldsymbol{\phi}_t$ and $\delta\phi_3$, respectively, and integrating by parts, the weak form of the above film system with two clamped edges can be derived as

$$\int_\Omega \left((\mathbf{S}_t^{(0)} + h\mathbf{S}_t^{(1)}) : \nabla\delta\boldsymbol{\phi}_t\right) \mathrm{d}A = 0, \tag{3.20}$$

$$2h\int_\Omega \left\{[(\mathbf{S}^{(0)} + h\mathbf{S}^{(1)})\mathbf{k} - (\mathbf{S}^{(0)} + h\mathbf{S}^{(1)})^{\mathrm{T}}\mathbf{k}] \cdot \nabla\delta\phi_3 - \frac{1}{3}h^2\mathbf{S}_t^{(1)} : \nabla\nabla\delta\phi_3\right\} \mathrm{d}A = 0, \tag{3.21}$$

where $\delta\boldsymbol{\phi} = (\delta\boldsymbol{\phi}_t, \delta\phi_3)$ is the virtual displacement, the symbol ":" denotes the trace of the product of two tensors, *i.e.*, $\mathbf{A} : \mathbf{B} = \mathrm{tr}(\mathbf{AB})$, and Ω represents the bottom surface of the film.

To solve the above weak form equations, we need the explicit expressions for $\mathbf{S}^{(0)}$ and $\mathbf{S}^{(1)}$ which can be obtained when a specific strain energy density function is given. Here the hyperelastic film is made of incompressible neo-Hookean material with the strain energy density

$$\psi = \frac{1}{2}\mu\left(\mathrm{tr}(\mathbf{F}\mathbf{F}^{\mathrm{T}}) - 3\right), \tag{3.22}$$

where μ denotes the shear modulus.

From (3.2) and (3.1), we have

$$\mathbf{S}^{(0)} = \mathcal{A}^{(0)}(\mathbf{F}^{(0)}) - p^{(0)}\mathcal{R}^{(0)}(\mathbf{F}^{(0)}), \tag{3.23}$$

where the moduli $\mathcal{A}^{(0)}$ and $\mathcal{R}^{(0)}$ are given by

$$\mathcal{A}^{(0)} = \mu(\mathbf{F}^{(0)})^{\mathrm{T}}, \quad \mathcal{R}^{(0)} = (\mathbf{F}^{(0)})^*, \tag{3.24}$$

in which $*$ denotes the adjoint of a tensor.

Similarly, from (3.2) and (3.1), we have

$$\mathbf{S}^{(1)} = \bar{\mathcal{A}}[\mathbf{F}^{(1)}] - p^{(1)}\mathcal{R}^{(0)}(\mathbf{F}^{(0)}), \tag{3.25}$$

where $\bar{\mathcal{A}}[\mathbf{F}^{(1)}]$ denotes the contraction of $\bar{\mathcal{A}}$ with $\mathbf{F}^{(1)}$, and $\bar{\mathcal{A}}$ is given by

$$\bar{\mathcal{A}} = \mathcal{A}^{(1)} - p^{(0)}\mathcal{R}^{(1)}, \tag{3.26}$$

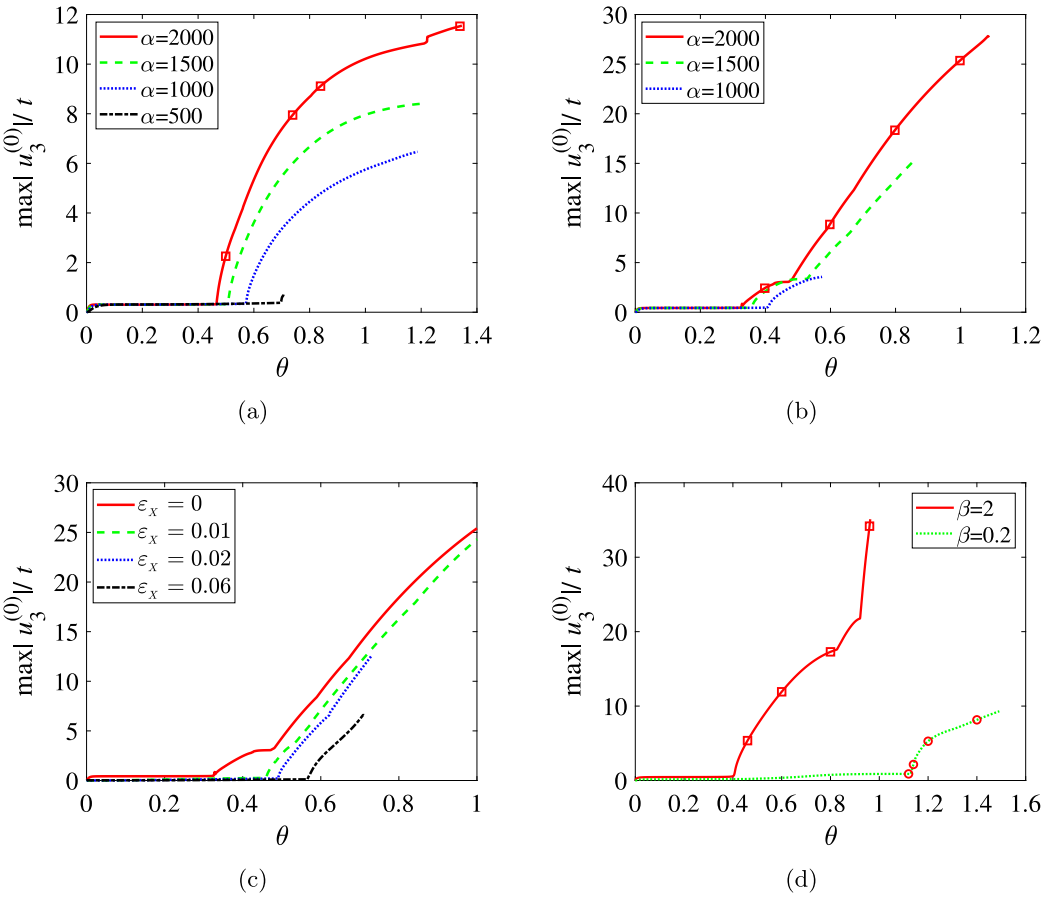


Fig. 3. Bifurcation diagrams of twisted films. (a) $\beta = 0.5$, (b) $\beta = 1$, (c) $\beta = 1$ and $\alpha = 2000$ with various pre-stretch ε_x, (d) $\alpha = 2000$.

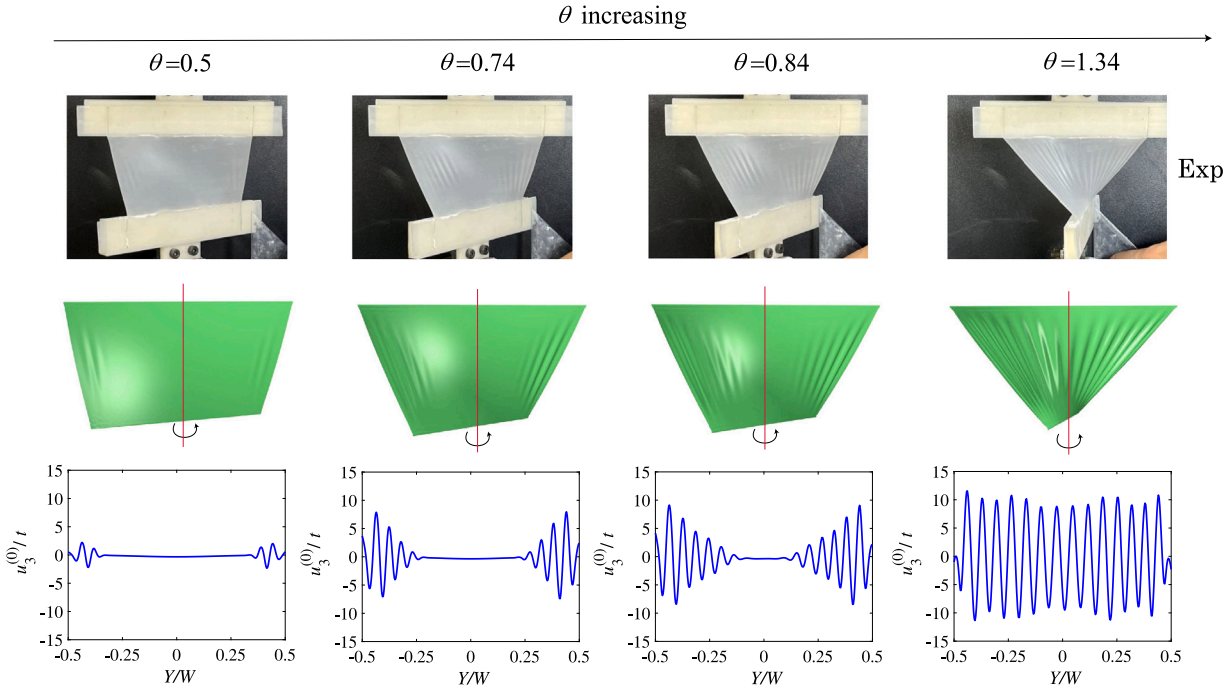


Fig. 4. Wrinkling evolution of twisted thin films with increasing angle $\theta = 0.5, 0.74, 0.84$ and 1.34. Wrinkles appear near both free ends and then develop toward the center upon further twisting. Geometric parameters: $\alpha = 2000$ and $\beta = 0.5$.

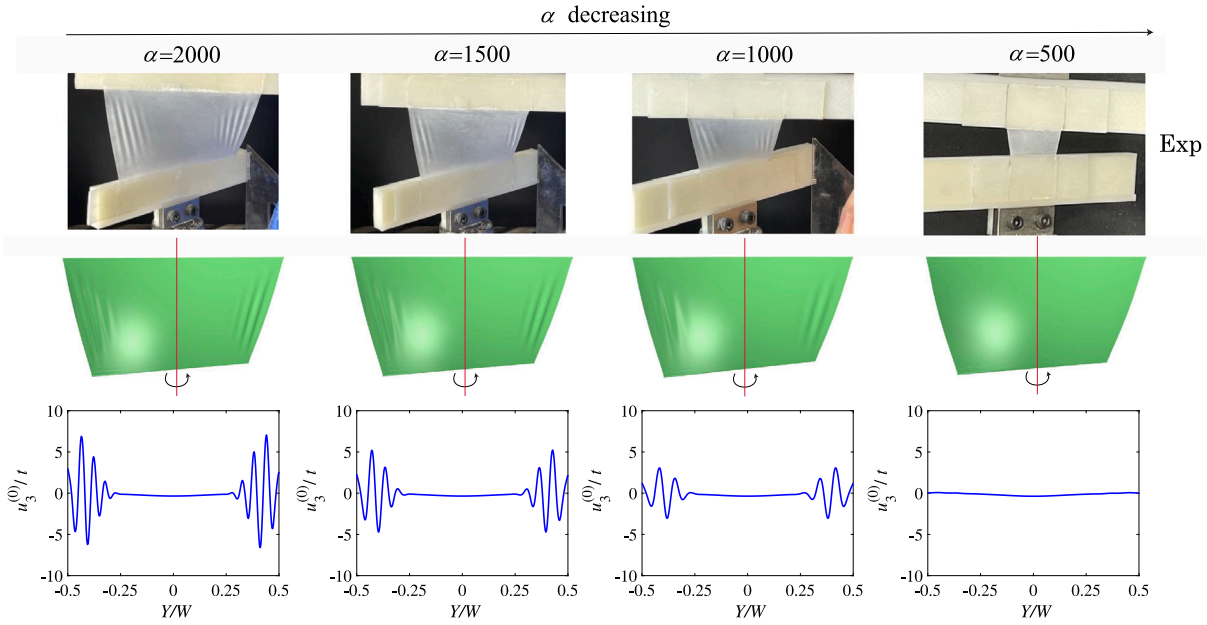


Fig. 5. Wrinkling morphology of thin films with different width/thickness ratios $\alpha = 2000, 1500, 1000$ and 500, twisted at $\theta = 0.68$. The rise of film thickness can resist wrinkles. Geometric parameter: $\beta = 0.5$.

in which the moduli $\mathcal{A}^{(1)}$ and $\mathcal{R}^{(1)}$ are respectively defined by

$$\mathcal{A}^{(1)} = \frac{\partial^2 \psi}{\partial \mathbf{F} \partial \mathbf{F}}(\mathbf{F}^{(0)}), \quad \mathcal{R}^{(1)} = \frac{\partial^2 R}{\partial \mathbf{F} \partial \mathbf{F}}(\mathbf{F}^{(0)}). \tag{3.27}$$

For the incompressible neo-Hookean material, the components of $\mathcal{A}^{(1)}$ and $\mathcal{R}^{(1)}$ are given by

$$\mathcal{A}^{(1)}_{ijkl} = \mu \delta_{ik} \delta_{jl}, \quad \mathcal{R}^{(1)}_{ijkl} = \frac{\partial F^*_{ij}}{\partial F_{lk}}|_{\mathbf{F}=\mathbf{F}^{(0)}}, \tag{3.28}$$

where δ_{ik} and δ_{jl} are the Krönecker delta symbols. Then we have

$$\mathbf{S}^{(1)} = \mu(\mathbf{F}^{(1)})^{\mathrm{T}} - p^{(0)} \mathcal{R}^{(1)}[\mathbf{F}^{(1)}] - p^{(1)}(\mathbf{F}^{(0)})^*. \tag{3.29}$$

We note that $p^{(0)}$ and $p^{(1)}$ can be obtained by combining the constraint Eq. (3.1) with Eq. (3.10) and the bottom traction free condition (3.14). From the coefficients of Z^0 and Z^1 of the series expansion of the constraint Eq. (3.1), we obtain

$$\mathbf{g} \cdot \mathbf{x}^{(1)} - 1 = 0, \tag{3.30}$$

and

$$\mathbf{g} \cdot \mathbf{x}^{(2)} + \mathcal{R}^{(0)} : \nabla \mathbf{x}^{(1)} = 0, \tag{3.31}$$

where

$$\mathbf{g} = \mathbf{x}^{(0)}_{,1} \wedge \mathbf{x}^{(0)}_{,2}, \tag{3.32}$$

in which the symbol $\wedge$ represents the cross product. Then, $p^{(0)}$ and $p^{(1)}$ can be obtained from (3.30) and (3.31), respectively.

Substituting (3.25) into Eq. (3.10) yields

$$\mathbf{x}^{(2)} = \frac{1}{\mu}(p^{(1)}\mathbf{g} - \mathbf{f}^{(2)}), \tag{3.33}$$

where

$$\mathbf{f}^{(2)} = \nabla \cdot \mathbf{S}^{(0)} - p^{(0)} \left(\mathcal{R}^{(1)}[\nabla \mathbf{x}^{(1)}] \right)^{\mathrm{T}} \mathbf{k}. \tag{3.34}$$

Then substituting (3.33) into (3.31), we have

$$p^{(1)} = \mathbf{x}^{(1)} \cdot \mathbf{f}^{(2)} - p^{(0)} \mathcal{R}^{(0)} : \nabla \mathbf{x}^{(1)}. \tag{3.35}$$

From (3.14) together with (3.23) and (3.24), it is easy to get

$$\mathbf{x}^{(1)} = \frac{1}{\mu} p^{(0)} \mathbf{g}. \tag{3.36}$$

Finally, $p^{(0)}$ can be obtained by substituting (3.36) into (3.30), which gives

$$p^{(0)} = \frac{\mu}{\mathbf{g} \cdot \mathbf{g}}. \tag{3.37}$$

In the following, we use the displacement $\mathbf{u} = \mathbf{x} - \mathbf{X}$ as the unknown with its series representation about the bottom surface of the film as below,

$$\mathbf{u} = \mathbf{u}^{(0)} + Z\mathbf{u}^{(1)} + Z^2\mathbf{u}^{(2)} + \cdots \tag{3.38}$$

in which

$$\mathbf{u}^{(0)} = \mathbf{x}^{(0)} - X\mathbf{e}_1 - Y\mathbf{e}_2, \quad \mathbf{u}^{(1)} = \mathbf{x}^{(1)} - \mathbf{k}, \quad \mathbf{u}^{(2)} = \mathbf{x}^{(2)}. \tag{3.39}$$

Through the above calculations, $\mathbf{S}^{(0)}$ and $\mathbf{S}^{(1)}$ are eventually expressed in terms of the bottom surface displacement $\mathbf{u}^{(0)}$. In the weak form (3.20) and (3.21), we set the virtual displacement $\boldsymbol{\phi} = \mathbf{u}^{(0)}$ and one obtains the following three equations in the weak form,

1. Equation for $\delta u_1^{(0)}$:

$$\int_\Omega \left((S^{(0)}_{11} + hS^{(1)}_{11})\delta u^{(0)}_{1,1} + (S^{(0)}_{21} + hS^{(1)}_{21})\delta u^{(0)}_{1,2} \right) \mathrm{d}A = 0, \tag{3.40}$$

2. Equation for $\delta u_2^{(0)}$:

$$\int_\Omega \left((S^{(0)}_{12} + hS^{(1)}_{12})\delta u^{(0)}_{2,1} + (S^{(0)}_{22} + hS^{(1)}_{22})\delta u^{(0)}_{2,2} \right) \mathrm{d}A = 0, \tag{3.41}$$

3. Equation for $\delta u_3^{(0)}$:

$$\int_\Omega \left(\left((S^{(0)}_{\alpha 3} - S^{(0)}_{3\alpha}) + h(S^{(1)}_{\alpha 3} - S^{(1)}_{3\alpha}) \right) \delta u^{(0)}_{3,\alpha} - \frac{1}{3} h^2 S^{(1)}_{\alpha\beta} \delta u^{(0)}_{3,\beta\alpha} \right) \mathrm{d}A = 0. \tag{3.42}$$

The wrinkling morphology evolutions of twisted thin films will be studied with the above weak forms together with proper boundary conditions numerically. As shown in Fig. 2(a), both ends of the film along $B'B$ and $C'C$ are clamped and twisted, while the other two ends are free. The distance between both clamped ends is kept constant during twisting. The boundary conditions for the weak form Eqs. (3.40)–(3.42)

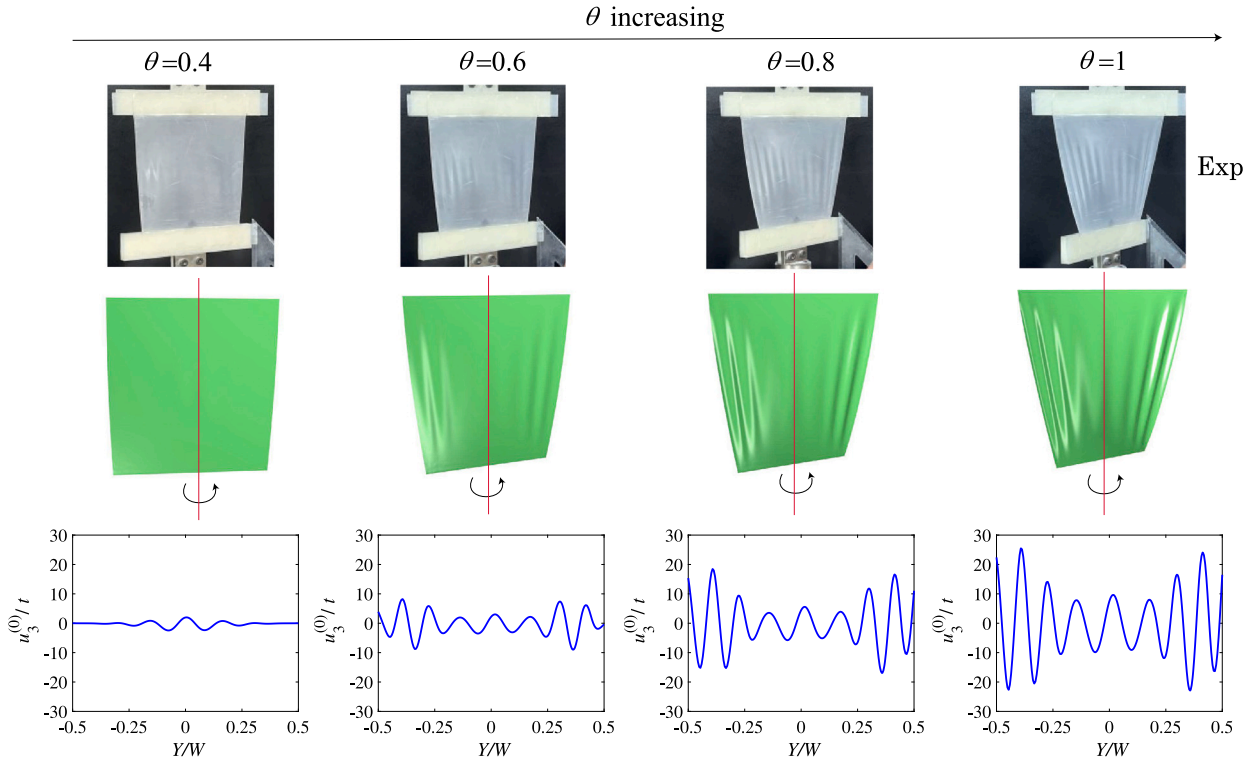


Fig. 6. Wrinkling evolution of a square film with increasing twisting angle $\theta = 0.4, 0.6, 0.8$ and 1. Wrinkles initially appear in the center of the film, and then spread toward both free ends. Geometric parameters: $\alpha = 2000$ and $\beta = 1$.

are given as

$$\begin{cases} u_1^{(0)} = 0, \quad \text{at} \quad C'C, B'B, \\ u_2^{(0)} = Y\left(\cos\left(\frac{1}{2}\theta\right) - 1\right), \quad \text{at} \quad B'B, C'C, \\ u_3^{(0)} = -Y\sin\left(\frac{1}{2}\theta\right), \quad \text{at} \quad B'B, \\ u_3^{(0)} = Y\sin\left(\frac{1}{2}\theta\right), \quad \text{at} \quad C'C, \\ \dfrac{\partial u_3^{(0)}}{\partial n} = 0, \quad \text{at} \quad B'B, C'C. \end{cases} \tag{3.43}$$

4. Results and discussion

We perform both twisting experiments and numerical simulations by implementing directly in COMSOL multiphysics the weak formulation (3.40)–(3.42), to explore buckling behavior and post-buckling evolutions of thin films subjected to torsion load. We examine the influence of aspect ratios, α and β, and pre-stretch on pattern formation, as it alters the effective stiffness of the thin film. Simultaneously, twisting experiment in the exact conditions is carried out to demonstrate the actual predictive capabilities of our model.

As transverse wrinkles are observed in twisting experiments, when the twisting angle θ is below its critical value, in the trivial and non-wrinkled state the deflection $u_3^{(0)}$ along the bottom center line $A'A$ (see Fig. 2(a)) remains small and not oscillating, while in the wrinkled state, the curve of $u_3^{(0)}$ along $A'A$ turns out to be oscillating. Hence, to detect the critical twisting angle, we take the maximum amplitude of $u_3^{(0)}$ along the line $A'A$ as a judgement criterion for the occurrence of wrinkles. In the following, we explore twist-induced wrinkles of thin films with various aspect ratios and identify different developing processes of wrinkles as the twisting angle increases.

Let us begin by considering a twisting film with aspect ratios $\beta = 0.5$ and $\alpha = 2000$. The pitchfork bifurcation curve is plotted in Fig. 3(a). As the twisting angle, θ, increases from zero, a minimal increase of the amplitude occurs initially, and then the amplitude remains almost unchanged until a critical twisting angle θ_{cr} beyond which the deflection increases dramatically. Evolutions of winkling morphology corresponding to the twisting angle at the red squares in the bifurcation diagram are illustrated in Fig. 4, where experimental wrinkling profiles are highly consistent with computations. When the torsion angle $\theta > \theta_{cr}$, wrinkles emerge near both free ends and then develop toward the center of the film upon further twisting. Finally, the whole thin film becomes a nearly uniform wrinkling configuration.

Bifurcation curves for thin films with different width/thickness ratios α are plotted in Fig. 3(a). One can see that the increase of the film thickness can increase the critical twisting angle and thus postpone the occurrence of wrinkles. Moreover, for the same twisting angle, the rise of film thickness can decrease wrinkling amplitudes. This fact is reasonable since the rise of film thickness strengthens the membrane and bending stiffness, and thus the film becomes more difficult to wrinkle. The experimental and numerical results of the wrinkled configurations at $\theta = 0.68$ with different width/thickness ratios α are given in Fig. 5, which shows a remarkable agreement between experimental observations and numerical predictions. Notably, the twisted thick film ($\alpha = 500$) is in a non-wrinkled state.

We next consider a square film ($\beta = 1$) under torsion. The similar pitch-fork bifurcation diagrams for thin films with different width/thickness ratios α are shown in Fig. 3(b). The experimental and computational wrinkling profiles corresponding to the twisting angle marked by red squares are depicted in Fig. 6. In contrast to the previous case, wrinkles initially appear in the center of the film and then spread toward both free ends, while the advanced wrinkles near both free ends have greater amplitudes than those in the center.

We then examine the effect of pre-tension ϵ_X on the twisted wrinkling. Bifurcation diagrams for different pre-stretches of the film with $\beta = 1$ and $\alpha = 2000$ are demonstrated in Fig. 3(c). We reveal that the critical wrinkling threshold increases as the pre-stretch increases, while the amplitudes of wrinkles decrease at the same twisting angle. Comparison between experimental observations and numerical predictions for different pre-stretches of the film at the twisting angle $\theta = 0.7$ is provided in Fig. 7. One can see that the pre-tension reduces the

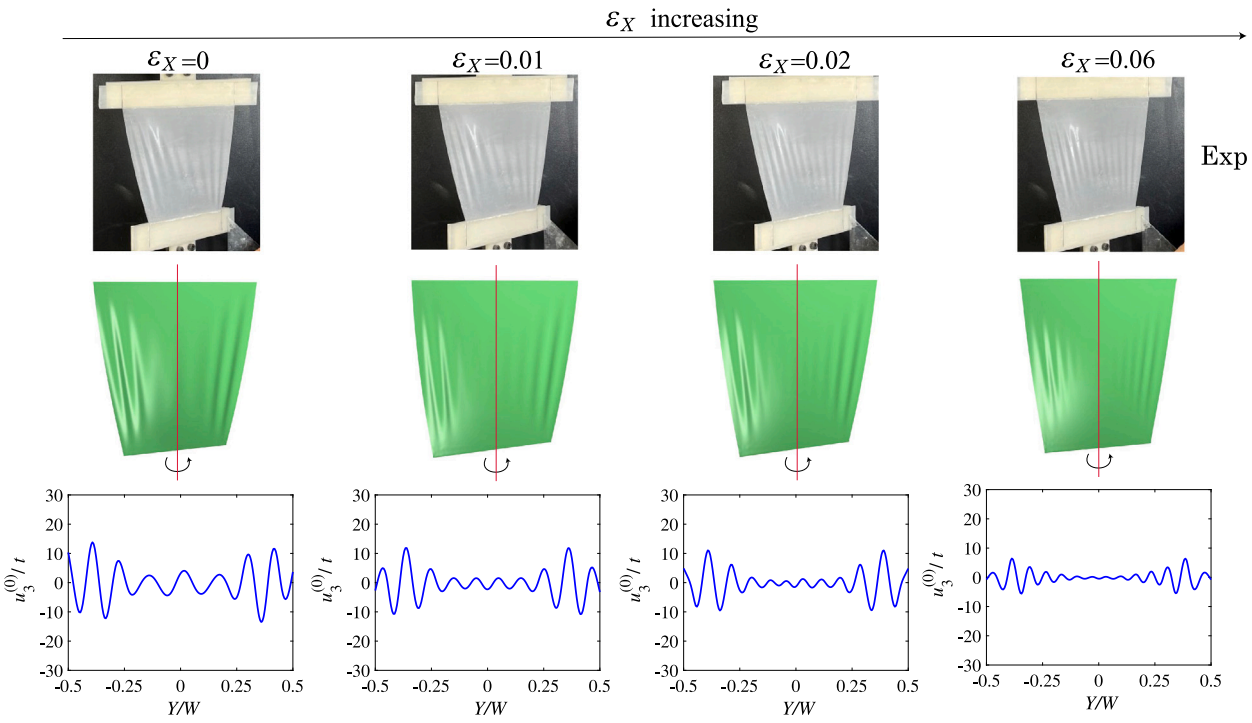


Fig. 7. Wrinkled configurations of twisted thin films ($\theta = 0.7$) with different pre-stretch ε_x. The rise of pre-tension increases film stiffness and thus can resist wrinkles. Geometric parameters: $\alpha = 2000$ and $\beta = 1$.

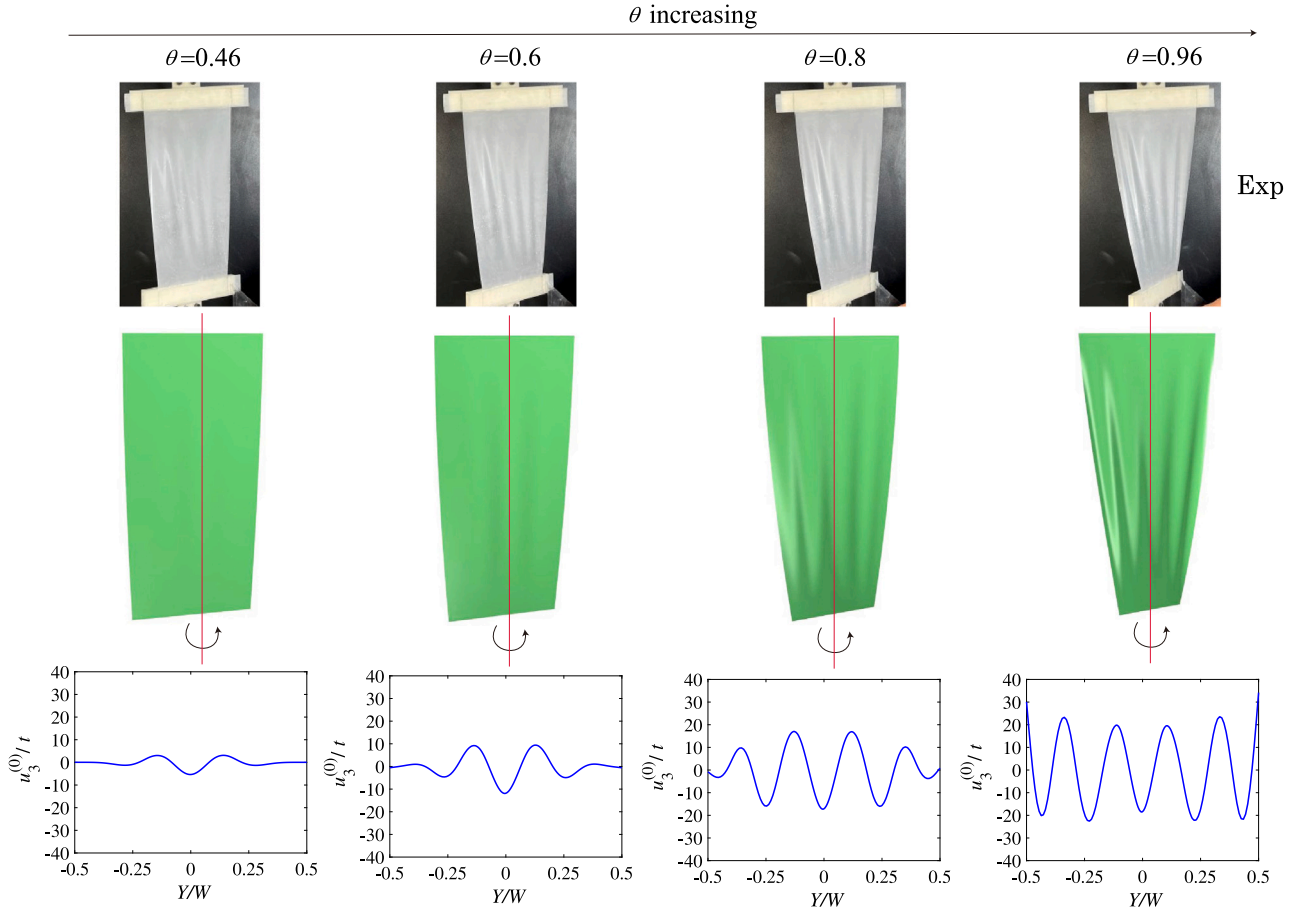


Fig. 8. Wrinkling evolution of a long thin film with increasing twisting angle $\theta = 0.46, 0.6, 0.8$ and 0.96. Geometric parameters: $\alpha = 2000$ and $\beta = 2$.

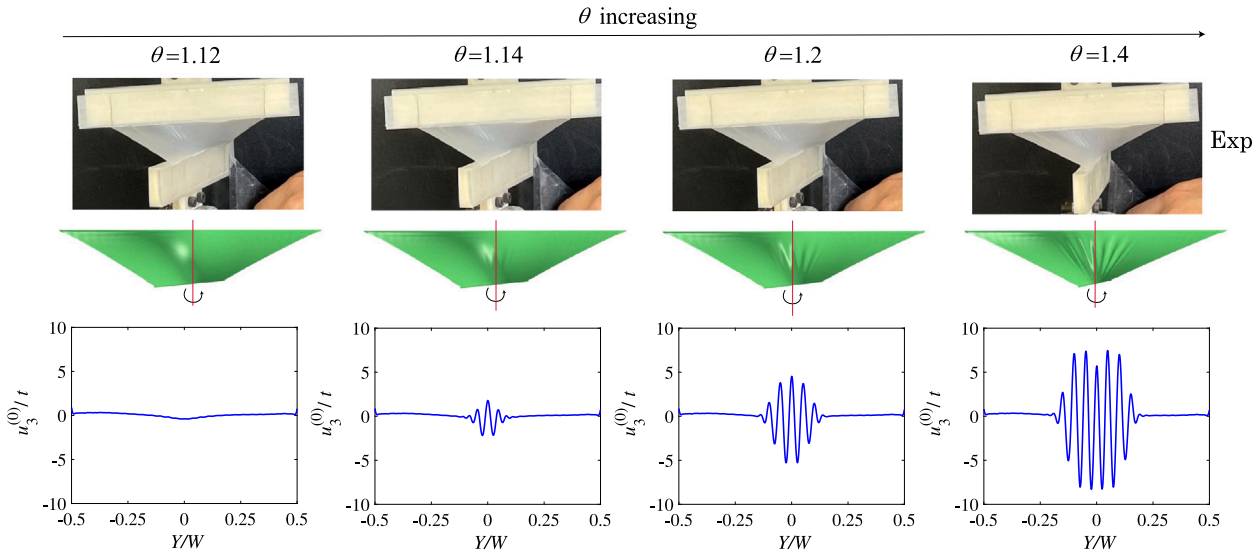


Fig. 9. Wrinkling evolution of a short thin film with increasing twisting angle $\theta = 1.12, 1.14, 1.2$ and 1.4. Wrinkles are localized in the film center. Geometric parameters: $\alpha = 2000$ and $\beta = 0.2$.

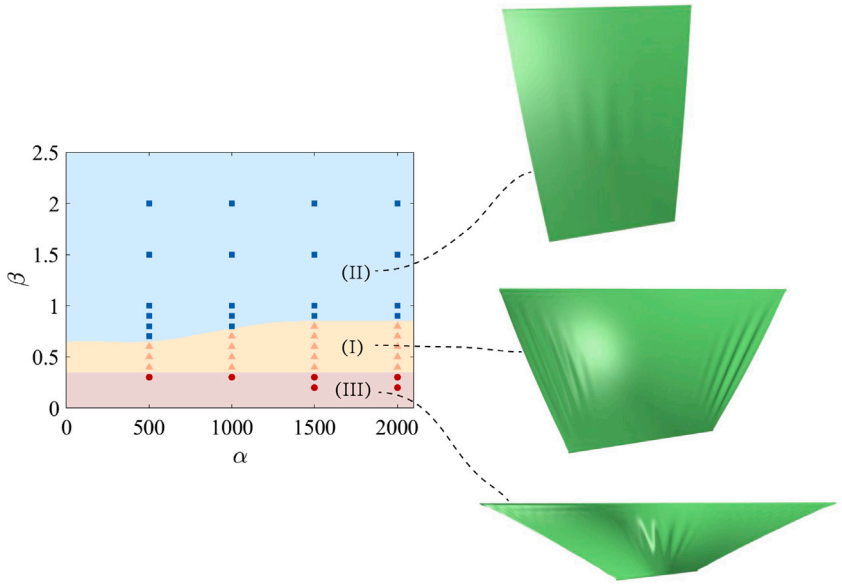


Fig. 10. Phase diagram of twisted thin films in a wide range of dimensions (length/width ratio β and width/thickness ratio α). Three distinguished wrinkling evolution regimes are identified.

wrinkling amplitudes and thus can smooth wrinkles, whereas the wave number is increased with the rise of pre-stretch.

We next investigate the effects of aspect ratios on pattern formation and evolution. Let us consider a relatively long thin film with $\beta = 2$ and $\alpha = 2000$ under twist. The bifurcation diagram and corresponding wrinkling scenario are respectively shown in Figs. 3(d) and 8, which exhibit similar pattern formation and evolution as the square film. We then account for a short thin film with $\beta = 0.2$ and $\alpha = 2000$ upon torsion. Compared with the previous three cases with $\beta = 0.5, 1$ and 2, the critical wrinkling threshold dramatically increases in short films, and the wrinkles are strictly localized in the film center and cannot develop to the free ends (see Fig. 9).

In summary, we uncovered three distinguished wrinkling scenarios of twisted films depending on aspect ratios: (I) wrinkles emerge at both free ends and then spread to the center; (II) wrinkles initially occur in the center and develop to both free ends in relatively long thin films; (III) wrinkles are constantly localized in the center in relatively short thin films. To provide an overall view of the wrinkling landscape and to quantitatively guide wrinkle-tunable design, we draw in Fig. 10 a phase diagram on pattern selection with respect to aspect ratios. For long films with length/width ratio $\beta > 0.9$, the wrinkling mode (II) prevails, while for short films with $\beta < 0.4$, the phase (III) dominates. The wrinkling mode (I) is more favorable in between ($0.4 < \beta < 0.9$), partially affected by width/thickness ratio for thick films with $\alpha < 1000$.

5. Conclusion

We have experimentally and numerically explored torsion-triggered wrinkling pattern formation and evolution of soft thin films. We developed a refined finite-strain plate model and then solved it by the finite element method via COMSOL. We uncovered three distinguished wrinkling scenarios of twisted thin films by a universal phase diagram: (I) wrinkles emerge at both free ends and then spread toward the center; (II) wrinkles occur in the center and develop toward both free

ends in relatively long thin films; (III) wrinkles are constantly localized in the center for relatively short thin films. Effects of aspect ratios and pre-stretch on wrinkling morphology were carefully examined, which reveals that the rise of film thickness and pre-tension can strengthen the film stiffness and thus increase the critical twisting threshold, leading to the prevention of wrinkle formation. The results may guide rational designs of wrinkle-tunable or wrinkle-resistant smart surfaces and membrane structures.

Declaration of competing interest

The authors declare that they have no known competing financial interests or personal relationships that could have appeared to influence the work reported in this paper.

Data availability

Data will be made available on request.

Acknowledgments

F.X. acknowledges the financial supports from the National Natural Science Foundation of China (Grants No. 12122204 and 11872150), Shanghai Pilot Program for Basic Research-Fudan University (Grant No. 21TQ1400100-21TQ010), Shanghai Shuguang Program (Grant No. 21SG05), and young scientist project of MOE innovation platform.

References

Chopin, J., Demery, V., Davidovitch, B., 2015. Roadmap to the morphological instabilities of a stretched twisted ribbon. J. Elasticity 119, 137–189.
Chopin, J., Kudrolli, A., 2013. Helicoids, wrinkles, and loops in twisted ribbons. Phys. Rev. Lett. 111, 174302.
Chopin, J., Romildo Filho, T.D., 2019. Extreme contractility and torsional compliance of soft ribbons under high twist. Phys. Rev. E 99, 043002.
Coman, C.D., Bassom, A.P., 2008. An asymptotic description of the elastic instability of twisted thin elastic plates. Acta Mech. 200, 59–68.
Crispino, D.J., Benson, R.C., 1986. Stability of twisted orthotropic plates. Int. J. Mech. Sci. 28, 371–379.
Dai, H.-H., Cai, Z.X., 2006. Phase transitions in a slender cylinder composed of an incompressible elastic material. I. Asymptotic model equation. Proc. R. Soc. Lond. Ser. A Math. Phys. Eng. Sci. 462, 75–95.
Dai, H.-H., Song, Z., 2014. On a consistent finite-strain plate theory based on three-dimensional energy principle. Proc. R. Soc. Lond. Ser. A Math. Phys. Eng. Sci. 470, 20140494.
Dai, H.-H., Wang, F.-F., 2012. Analytical solutions for the post-buckling states of an incompressible hyperelastic layer. Anal. Appl. 10, 21–46.
Dai, H.-H., Wang, Y., Wang, F.-F., 2013. Primary and secondary bifurcations of a compressible hyperelastic layer: Asymptotic model equations and solutions. Int. J. Non-Linear Mech. 52, 58–72.
Dai, H.-H., Wang, F.-F., Wang, J., Xu, J., 2015. Pitchfork and octopus bifurcations in a hyperelastic tube subjected to compression: Analytical post-bifurcation solutions and imperfection sensitivity. Math. Mech. Solids 20, 25–52.
Faghfouri, S., Rammerstorfer, F.G., 2020. Mode transitions in buckling and post-buckling of stretched–twisted strips. Int. J. Non-Linear Mech. 127, 103609.
Goriely, A., Nizette, M., Tabor, M., 2001. On the dynamics of elastic strips. J. Nonlinear Sci. 11, 3–45.
Green, A.E., 1936. The equilibrium and elastic stability of a thin twisted strip. Proc. R. Soc. Lond. Ser. A Math. Phys. Eng. Sci. 154, 430–455.
Green, A.E., 1937. The elastic stability of a thin twisted strip. II. Proc. R. Soc. Lond. Ser. A Math. Phys. Eng. Sci. 161, 197–220.
Healey, T.J., Li, Q., Cheng, R.-B., 2013. Wrinkling behavior of highly stretched rectangular elastic films via parametric global bifurcation. J. Nonlinear Sci. 23, 777–805.
Huang, Z., Hao, Y., Li, Y., Hu, H., Wang, C., Nomoto, A., Pan, T., Gu, Y., Chen, Y., Zhang, T., Li, W., Lei, Y., Kim, N., Wang, C., Zhang, L., Ward, J.W., Maralani, A., Li, X., Durstock, M.F., Pisano, A., Lin, Y., Xu, S., 2018. Three-dimensional integrated stretchable electronics. Nature Electron. 1, 473–480.
Kohn, R.V., O'Brien, E., 2018. The wrinkling of a twisted ribbon. J. Nonlinear Sci. 28, 1221–1249.
Kudrolli, A., Chopin, J., 2018. Tension-dependent transverse buckles and wrinkles in twisted elastic sheets. Proc. R. Soc. Lond. Ser. A Math. Phys. Eng. Sci. 474, 20180062.
Li, Q., Healey, T.J., 2016. Stability boundaries for wrinkling in highly stretched elastic sheets. J. Mech. Phys. Solids 97, 260–274.
Mockensturm, E.M., 2001. The elastic stability of twisted plates. ASME J. Appl. Mech. 68, 561–567.
Nayyar, V., Ravi-Chandar, K., Huang, R., 2011. Stretch-induced stress patterns and wrinkles in hyperelastic thin sheets. Int. J. Solids Struct. 48, 3471–3483.
Sipos, A.A., Fehér, E., 2016. Disappearance of stretch-induced wrinkles of thin sheets: A study of orthotropic films. Int. J. Solids Struct. 97–98, 275–283.
Wang, F.-F., Dai, H.-H., Giorgio, I., 2022a. A numerical comparison of the uniformly-valid asymptotic plate equations with a 3D model: Clamped rectangular incompressible elastic plates. Math. Mech. Solids 27, 1370–1396.
Wang, T., Fu, C., Xu, F., Huo, Y., Potier-Ferry, M., 2019a. On the wrinkling and restabilization of highly stretched sheets. Internat. J. Engrg. Sci. 136, 1–16.
Wang, J., Song, Z., Dai, H.-H., 2016. On a consistent finite-strain plate theory for incompressible hyperelastic materials. Int. J. Solids Struct. 78–79, 101–109.
Wang, F.-F., Steigmann, D.J., Dai, H.-H., 2019b. On a uniformly-valid asymptotic plate theory. Int. J. Non-Linear Mech. 112, 117–125.
Wang, T., Yang, Y., Xu, F., 2022b. Mechanics of tension-induced film wrinkling and restabilization: A review. Proc. R. Soc. Lond. Ser. A Math. Phys. Eng. Sci. 478, 20220149.
Wong, Y., Pellegrino, S., 2006. Winkled membranes. Part I: Experiments. J. Mech. Mater. Struct. 1, 3–25.
Zheng, L., 2009. Wrinkling of Dielectric Elastomer Membranes (Ph.D. thesis). California Institute of Technology, Pasadena, CA.